Numerical Studies on Dynamic Load Testing of an Open-ended Pipe Pile and a Case Study

L. Phan Ta[1], T. Matsumoto[2] and H. Nguyen Hoang[3]
[1]*Department of Construction, HCMC University of Architecture, Ho Chi Minh city, Viet Nam*
[2]*Graduate School of Natural Science and Technology, Kanazawa, Japan*
[3]*South VietNam Bridge Road Building Technology Institute, Viet Nam*
[1]*E-mail*: phantale@hcmuarc.edu.vn

ABSTRACT: This paper proposes a numerical approach using a matrix form with Newmark's β method to analyse the phenomenon of the one-dimensional stress-wave propagation in an open-ended pipe pile with the aim of enhancing the reliability of the dynamic analysis. To verify the proposed method, first, the calculated results obtained from the proposed method were compared with those obtained from the rigorous continuum method FLAC^{3D}, the conventional Smith method, and the theoretical solution. The calculated results obtained from the proposed method were in good agreement with those obtained from the continuum method FLAC^{3D}. Second, static and dynamic load tests of a spun concrete pile in a construction site in Viet Nam were carried out. Wave Matching Analyses (WMAs) using the proposed method were conducted to derive a static load-displacement curve. The derived curve was comparable to that measured in static load test (SLT), indicating that the proposed method has high potential to predict the static pile response. Hence, the proposed method could be used as a practical alternative to the conventional SLT.

1. INTRODUCTION

Open-ended steel pipe piles have been used for years as the primary solution to constructing foundations for various structures in offshore conditions. Recently, there has been an increasing interest in using spun (pre-stressed concrete) piles for the foundations of many structures, especially residential and industrial buildings. During driving such piles into the ground, a part of the soil around the pile toe enters into the pile to create a soil column called a soil plug. Depending on the relative movement between the pile and the soil plug, the pile is said to be plugged, partially plugged or unplugged. In all three cases, the total resistance of an open-ended pipe pile is the summation of outer shaft resistance, soil plug resistance (or inner shaft resistance) and pile tip resistance.

In pile foundation design, it is common to use the static load-displacement relation of a single pile to determine its bearing capacity and corresponding displacement. At present, the load-displacement relation is directly obtained from a static load test (SLT) or derived from the interpretation of dynamic load test (DLT) or rapid load test (RLT) signals. While the SLT is considered the most reliable method, it is costly and time-consuming. Rapid pile load testing methods, such as the Statnamic load test method (Bermingham et al. 1989) and the Spring-hammer load test method (Matsumoto et al. 2004) in which the phenomenon of stress-wave propagation in piles could be ignored, have been developed. Various methods of interpreting the measured dynamic signals, such as the unloading point method (UPM) (Kusakabe et al. 1995) and the non-linear damping method (NLDM) (Matsumoto et al. 1994) have been proposed to derive the static load-settlement relation of the piles. In the DLT, wave matching analysis (WMA) plays a key role in identifying soil resistance parameters which are then used to estimate the static load-displacement relation. Such analysis requires an appropriate numerical method and numerical analysis model as well. Conventionally, the Smith method (Smith, 1960), the characteristic solution and the finite difference scheme of the one dimensional wave equation have been employed for wave matching analysis. For example, the Smith method is employed in WEAP and CAPWAP (Goble et al. 1977, 1979), characteristic solutions are adopted in TNOWAVE (Middendorp et al. 1986) and KWAVE (Matsumoto et al. 1991), and the finite difference scheme is used in KWAVE-FD (Wakisaka et al. 2004).

In the case of open-ended pipe piles, it is necessary to consider the inner shaft resistance, as well as the wave propagation in the soil plug, in a wave matching analysis. Heerema and de Jong (1979) used the pile-in-pile model with Smith's empirical soil models to analyse the stress wave propagation in an open-ended pile. They were followed by Randolph and Simon (1986), Matsumoto et al. (1991), and Randolph and Deeks (1992) who used rational soil models with linear soil stiffness and a damping coefficient for pile driving analyses.

Considering numerical methods based on the one-dimensional stress-wave propagation theory, their advantage is rapid calculation. Nevertheless, the characteristic solution and the Smith method may have numerical instability when soil stiffness and the velocity-dependent resistance have large values. One of the reasons is that the displacement and velocity of a pile node at the previous calculation time step are used to calculate the soil resistance mobilised at the present calculation step. In other words, the pile behaviour and soil resistance are not fully coupled at each time step. This aspect will be discussed in detail later through a comparison of calculation results using the Smith method and a rigorous numerical method.

More rigorous methods, in which the soil surrounding a pile is regarded as a continuum medium using the finite element method or the finite difference method, have been developed. Chow and Smith (1984) performed axisymmetric finite element analyses for solid and pipe piles driven into clay under undrained conditions. Liyanapathirana et al. (2001) studied the driving responses at the vicinity of the pile tip of thin walled open-ended pipe piles using a two-dimensional axisymmetric finite element method. The results indicated that the shear stress reached the maximum magnitude right above the bottom of the soil plug while the vertical stress wave reached the highest magnitude beneath the bottom of the soil plug. Thus, the interaction between the waves travelling in radial and vertical directions at the bottom of the soil plug was considerable. Paikowsky and Chernauskas (2008) employed a two-dimensional finite difference scheme to investigate the spatial stress generated within a soil plug. They suggested that radial wave propagation within the soil plug, as well as compression wave propagation within the pile and the soil plug, should be taken into account. Although such continuum methods are regarded as the most rigorous methods in pile driving analysis, they are relatively slow in calculation, with runtimes of several hours. Therefore, it is currently not practical to apply continuum methods in routine pile dynamic analysis.

In order to overcome the above shortcomings of conventional one-dimensional stress-wave propagation analyses as well as those of the rigorous continuum methods, the matrix method of one-dimensional stress-wave propagation analysis in a pile using rational soil models recommended by Randolph and Deeks (1992) is

proposed in this paper. In the proposed method, displacements, velocities and accelerations of the pile, the outer soil and the inner soil at all the nodes are calculated simultaneously, and the soil stiffness- and velocity-dependent resistances are calculated at the same calculation step. Influence of the stress wave propagation on the soil plug is taken into account for an open-ended pile. Furthermore, the non-linearity of soil stiffness and the radiation damping in the soil models are considered. The proposed method can also be used for the analysis of the static loading of a pile, if the damping and inertia of the pile and the soil are ignored. To verify the proposed method, first, the calculated results obtained from the proposed method were compared with those from the theoretical solution, the conventional Smith method, and a continuum method using a well-known three-dimensional explicit finite-difference computer program, FLAC^{3D}. Second, the proposed method was used to analyse field data from dynamic and static load tests of a spun concrete pile in a construction site in Viet Nam.

2. NUMERICAL STUDIES

2.1 Proposed numerical model with rational soil models

The numerical model employed for analysing the stress wave propagation in an open-ended pipe pile is shown in Figure 1. In this model, the pile and the soil plug are modelled as a series of massless linear springs with discrete masses at the nodes. Outer frictional forces acting on the pile nodes as well as inner frictional forces acting between the soil plug nodes and the pile nodes are considered. That is, we have four degrees of freedom (pile, soil plug, outer soil and inner soil) at each pile level. In the proposed numerical model, the soil reaction on the pile annulus and the soil reaction beneath the soil plug are separately considered. The rational soil models proposed by Randolph and Deeks (1992) are implemented in the proposed numerical model for both outer and inner soil resistance.

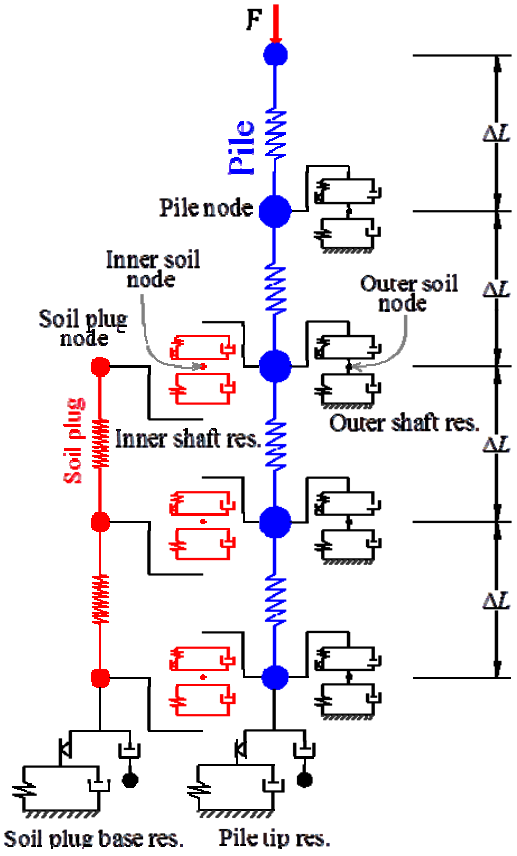

Figure 1 Pile – soil system

Figures 2 and 3 show the rational soil models employed in the proposed method. In Figure 2, u_p and v_p are the displacement and the velocity at the pile node, and u_s and v_s are those at the adjacent soil node, respectively. The outer shaft resistance, R_m, at the pile node, m, is calculated as:

$$R_m = (k_s u_s + c_r v_s) \cdot 2\pi r_o \cdot \Delta L \tag{1}$$

where k_s and c_r are the soil spring stiffness and the damping, respectively, and r_o is the outer radius of pile. These values can be approximately estimated using the following equations (Randolph and Deeks, 1992):

$$k_s = \frac{2.75G}{2\pi r_o} \tag{2}$$

$$c_r = \sqrt{\rho_s G} \tag{3}$$

in which G and ρ_s are the shear modulus and density of the soil, respectively.

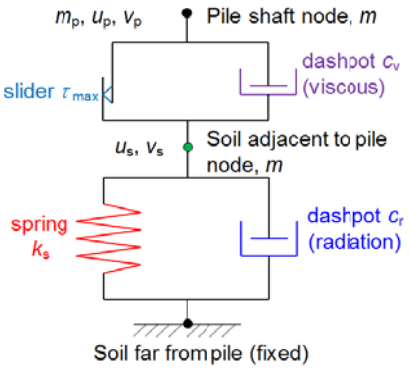

Figure 2 Shaft soil model

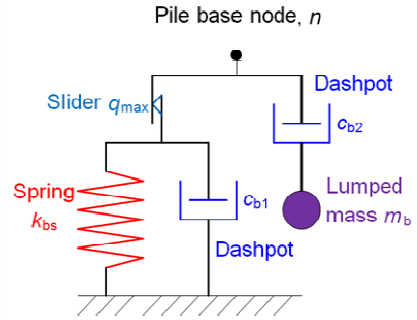

Figure 3 Base soil model

Under static loading conditions, the soil stiffness in the shaft soil model, $k_{s(static)}$, which is lower than that under dynamic loading conditions, is estimated using the following equations provided by Randolph and Deeks (1992).

$$k_{s(static)} = \frac{G}{\zeta r_o} \tag{4}$$

$$\zeta = \ln \frac{2.5L_e(1-\nu)}{r_o} \tag{5}$$

in which L_e is the embedment pile length.

The base resistance beneath the pile tip (annular section), R_p, and beneath the soil plug, R_{sp}, are calculated by the following equations:

$$R_p = \left[(k_{b\text{-}p} u_{bs\text{-}p} + c_{b1} v_{bs\text{-}p}) + c_{b2}(v_p - v_{bw\text{-}p}) \right] \pi (r_o^2 - r_i^2) \tag{6}$$

$$R_{sp} = \left[(k_{b\text{-}sp} u_{bs\text{-}sp} + c_{b1} v_{bs\text{-}sp}) + c_{b2} (v_{sp} - v_{bw\text{-}sp}) \right] \pi r_i^2 \quad (7)$$

In Eq. (6), $k_{b\text{-}p}$ is the spring stiffness, c_{b1} and c_{b2} are the damping factors, $u_{bs\text{-}p}$ and $v_{bs\text{-}p}$ are the displacement and velocity of the soil beneath the pile tip, $v_{bw\text{-}p}$ is the velocity of the additional soil mass and $m_{bw\text{-}p}$ is the additional soil mass of the soil resistance model beneath the pile tip. Those for the soil resistance beneath the soil plug are indicated with the suffix "sp" in Eq. (7). And, r_o and r_i are the outer and inner radii of the pile. These values are also approximated as follows (Randolph and Deeks, 1992):

$$k_{b\text{-}p} = \frac{4G}{\pi (r_o + r_i)(1-\nu)} \quad (8)$$

$$k_{b\text{-}sp} = \frac{4G}{\pi r_i (1-\nu)} \quad (9)$$

$$c_{b1} = c_{b2} = \frac{3.2}{\pi (1-\nu)} \sqrt{G \rho_s} \quad (10)$$

$$m_{bw\text{-}p} = 16 (r_o - r_i) \frac{0.1 - \nu^4}{\pi (1-\nu)} \rho_s \quad \text{(per unit area)} \quad (11)$$

$$m_{bw\text{-}sp} = 16 r_i \frac{0.1 - \nu^4}{\pi (1-\nu)} \rho_s \quad \text{(per unit area)} \quad (12)$$

where ν is the Poisson's ratio of the base soil.

In the rational shaft resistance model, the maximum dynamic soil resistance at the pile-outer soil interface, $\tau_{max\_out}^{dyn}$, and at the pile-inner soil interface, $\tau_{max\_in}^{dyn}$, are calculated by the following equations:

$$\tau_{max\_out}^{dyn} = \tau_{max\_out} \left[1 + \alpha \left(\frac{\dot{w}_p - \dot{w}_{so}}{v_o} \right)^{\beta} \right] \quad \text{(for outer interface)} \quad (13)$$

$$\tau_{max\_in}^{dyn} = \tau_{max\_in} \left[1 + \alpha \left(\frac{\dot{w}_p - \dot{w}_{si}}{v_o} \right)^{\beta} \right] \quad \text{(for inner interface)} \quad (14)$$

where τ_{max_out} and τ_{max_in} are the maximum static shaft resistances at the outer and inner interfaces. $\dot{w}_p$, $\dot{w}_{so}$, and $\dot{w}_{si}$ are the velocities of the pile, the outer, and the inner soil nodes, respectively. v_0 is a reference velocity (= 1 m/s for convenience). α varies from 0.1 (for sand) to unity (for clay) and β = 0.2 (for all soils) (Randolph and Deeks, 1992).

The mobilised outer and inner shaft resistances, $\tau_{mob\text{-}out}$ and $\tau_{mob\text{-}in}$, are calculated by:

$$\tau_{mob\_out} = k_{so} w_{so} + c_{ro} \dot{w}_{so} \quad (15)$$

$$\tau_{mob\_in} = k_{si} (w_{si} - w_{sp}) + c_{ri} (\dot{w}_{si} - \dot{w}_{sp}) \quad (16)$$

where, k_{so} and k_{si} are the spring stiffnesses, c_{ro} and c_{ri} are the radiation dampings of the outer and inner soil, respectively. w_{so}, w_{si}, and w_{sp} are the displacements of the outer soil, inner soil, and soil plug, respectively. $\dot{w}_{sp}$ is the velocity of the soil plug node.

If the absolute value of the mobilised soil resistance exceeds the corresponding maximum dynamic soil resistance at the interface, slippage occurs, resulting in relative displacements between the pile and the soil.

To take into account the non-linearity of the soil stiffness shown in Figure 4, the empirical relation introduced by Chow (1986) is used in the proposed method to calculate the soil stiffness in the loading stage at the pile shaft, k_s, or at the pile tip, k_b, in the current step from the initial values, $k_{s\text{-}ini}$ or $k_{b\text{-}ini}$, as follows:

$$k_s = k_{s\text{-}ini} \left(1 - R_{fs} \frac{\tau}{\tau_{max}^{pos} \text{ or } \tau_{max}^{neg}} \right) \quad (17)$$

$$k_b = k_{b\text{-}ini} \left(1 - R_{fb} \frac{q_b}{q_{max}^{comp} \text{ or } q_{max}^{tens}} \right) \quad (18)$$

in which, R_{fs}, τ, τ_{max}^{pos} and τ_{max}^{neg} are the non-linearity coefficient, mobilised static soil resistance, positive maximum shear resistance (upward friction to the pile shaft) and negative maximum shear resistance (downward friction to the piles haft) at the pile shaft, respectively. R_{fb}, q_b, q_{max}^{comp} and q_{max}^{tens} are the non-linearity coefficient, mobilised static soil resistance, end-bearing resistance in compression and end-bearing resistance in tension at the pile tip, respectively. For the unloading and reloading stages, the initial soil stiffness was used to calculate the soil response.

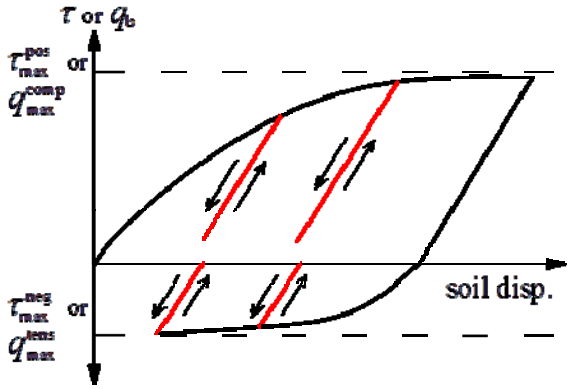

Figure 4 Non-linear soil responses

In the case of a non-linear behaviour of the soil stiffness, k_s or k_b, it may be appropriate to consider non-linear damping. According to Eq. (2) and Eq. (3) or Eq. (8), Eq. (9), and Eq. (10), non-linearity is related to the reduction of the shear modulus, G, of the soil. Hence, based on the above equations as well as Eq. (17) and Eq. (18), the following non-linear damping is considered:

$$c_r = \left(1 - R_{fs} \frac{\tau}{\tau_{max}^{pos} \text{ or } \tau_{max}^{neg}} \right)^{0.5} c_{r\text{-}ini} \quad (19)$$

$$c_{b1} = c_{b2} = \left(1 - R_{fb} \frac{q_b}{q_{max}^{comp} \text{ or } q_{max}^{tens}} \right)^{0.5} c_{b\text{-}ini} \quad (20)$$

where $c_{r\text{-}ini}$ and $c_{b\text{-}ini}$ are the initial values of c_r and $c_{br1} = c_{br2}$, respectively.

In order to calculate the responses of the outer and inner soils at the same time as the responses of the pile and the soil plug, a plastic slider in the rational soil models is connected to an interface spring

with a great enough stiffness to minimise the relative displacement between the pile and the adjacent soil before slippage.

2.2. Formulation of calculations

By writing the force equilibrium equation at each pile node, soil plug node, outer soil node, and inner soil node, the pile motion can be expressed by the well-known matrix form as follows:

$$[K]\{w\}+[C]\{\dot{w}\}+[M]\{\ddot{w}\}=\{F\} \tag{21}$$

in which [*K*], [*C*] and [*M*] are the global stiffness, damping, and mass matrices, respectively. $\{w\}$, $\{\dot{w}\}$, $\{\ddot{w}\}$ and $\{F\}$ are the displacement, velocity, acceleration and the applied force vectors, respectively. Such matrix form calculation scheme was first used in geotechnical engineering by Idriss and Seed (1969) to calculate the seismic response of horizontal soil layers.

Matrix [*K*] consists of the spring stiffness of the pile, the soil plug, the interface spring, the outer shaft soil, the inner shaft soil, the base soil beneath the pile tip and the soil plug base. If a slip failure occurs at a node, the value of the interface spring stiffness, k_{inter}, is set to zero at that node. When the pile and the soil re-join, the value of the interface spring stiffness is recovered.

Matrix [*C*] includes the damping values of the outer shaft soil, the inner shaft soil, the base soil, and the additional soil masses. Matrix [*M*] involves the mass of each pile node, the mass of each soil plug node, and the mass of additional soil masses beneath the pile tip and the soil plug base.

From the Newmark's β method (Newmark, 1959), the acceleration, $\{\ddot{w}\}_{t+\Delta t}$, and the velocity, $\{\dot{w}\}_{t+\Delta t}$, at the current time, $t+\Delta t$, can be given by the following equations using $\{w\}_{t+\Delta t}$ for the current step, and $\{w\}_t$, $\{\dot{w}\}_t$ and $\{\ddot{w}\}_t$ for the previous step:

$$\{\dot{w}\}_{t+\Delta t}=\frac{\gamma}{\beta\Delta t}\left(\{w\}_{t+\Delta t}-\{w\}_t\right)+\left(1-\frac{\gamma}{\beta}\right)\{\dot{w}\}_t+\frac{\Delta t}{2}\left(2-\frac{\gamma}{\beta}\right)\{\ddot{w}\}_t \tag{22}$$

$$\{\ddot{w}\}_{t+\Delta t}=\frac{\{w\}_{t+\Delta t}-\{w\}_t}{\beta\Delta t^2}-\frac{\{\dot{w}\}_t}{\beta\Delta t}-\left(\frac{1}{2\beta}-1\right)\{\ddot{w}\}_t \tag{23}$$

in which, γ = 1/2 and β varies from 0 to 1 (β = 1/4 for the constant average acceleration method, and β = 1/6 for the linear acceleration method). β = 1/6 was adopted in the proposed method because of its high accuracy (Edward, 2000) in short time intervals.

Using these above equations, the incremental form of Eq. (21) is rewritten as below:

$$\left[[K]_t+\frac{[C]_t}{2\beta\Delta t}+\frac{[M]_t}{\beta\Delta t^2}\right]\{\Delta w\}_{t+\Delta t}= \left[\{F\}_{t+\Delta t}-\sum_0^t[K]_t\{\Delta w\}_t\right]+\left[\left(\frac{1}{2\beta}-1\right)[C]_t+\frac{[M]_t}{\beta\Delta t}\right]\{\dot{w}\}_t +\left[\left(\frac{1}{2\beta}-2\right)\frac{\Delta t}{2}[C]_t+\left(\frac{1}{2\beta}-1\right)[M]_t\right]\{\ddot{w}\}_t \tag{24}$$

The coefficient terms of the matrix in the left hand side of Eq. (24) are known. Therefore, the increment of the displacement vector, $\{\Delta w\}_{t+\Delta t}$, for the pile, soil plug, outer soil, and inner soil can be solved readily. Using these results, the total displacement vector $\{w\}_{t+\Delta t}$ at the current step is calculated by Eq. (25):

$$\{w\}_{t+\Delta t}=\{w\}_t+\{\Delta w\}_{t+\Delta t} \tag{25}$$

The velocities and accelerations are then promptly derived from Eqs. (22) and (23). Note that $[K]_t$ and $[C]_t$ matrices are updated in each calculation step while $[M]_t$ matrix remains unchanged.

If the values of [*C*] and [*M*] are set at zero, the above approach can be applied to a fully static situation.

More detail explanation of the calculation procedure is presented in Appendix with substantial assemblies of [*K*], [*C*] and [*M*].

2.3. Verification of the proposed method

2.3.1 Comparison with theoretical solution

A homogeneous pile without soil resistance subjected to a vertical triangle impact force was calculated using the proposed numerical method. The calculated results were then compared with the theoretical values. The properties of the pile and the impact force are shown in Figure 5.

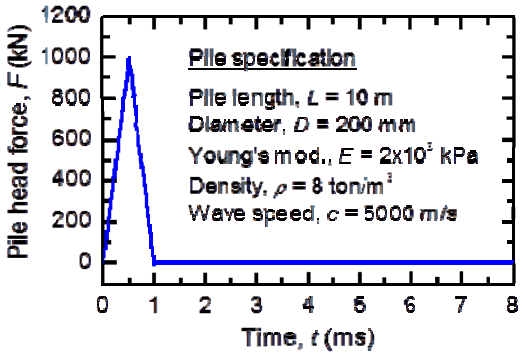

Figure 5 Head force and specification of the pile

The pile was divided into 50 elements in order to have a pile element length, ΔL, of 0.2 m, and the time step was set at $4\Delta t_{cri}$, $3\Delta t_{cri}$, $2\Delta t_{cri}$, $1\Delta t_{cri}$, $0.5\Delta t_{cri}$ and $0.2\Delta t_{cri}$ in order to evaluate the stability of Newmark's β approach, which is used in the proposed method. Here, Δt_{cri} is defined as $(\Delta L/c)/2$ where c is the theoretical bar wave velocity, $c=\sqrt{E/\rho}$. When time steps were greater than $2\Delta t_{cri}$, a solution could not be obtained.

Figures 6a and 6b compare the theoretical solutions and the results calculated from the proposed method, respectively, for the axial force and the velocity versus time at the middle point of the pile (z = 5 m). Although a good agreement between the theoretical and calculated results can be seen in both figures for the different time steps, the calculation results using $\Delta t = 0.5\Delta t_{cri}$ gave the solutions which were the closest to the theoretical values in the figures. The calculation results using $\Delta t = 0.2\Delta t_{cri}$ were almost equal to those using $\Delta t = 0.5\Delta t_{cri}$. Hence, $\Delta t = 0.5\Delta t_{cri}$ was used in the proposed method in order to achieve an acceptable accuracy and shorter calculation time.

It should be noted that the above verification was conducted for a pile without soil resistance. No theoretical solution is available for wave propagation in a pile with soil resistance. Hence, the proposed approach is further verified for a pile with soil resistance in the following part.

2.3.2 Comparison with the Smith method

In order to compare the calculated results obtained from the proposed method with those from the Smith method in which rational soil models were employed, an open-ended pipe pile having a length, *L*, of 21 m and a wave speed, *c*, of 4000 m/s in a uniform ground with the specifications as shown in Figure 7 was analysed. The pile was divided into 42 elements for the two methods, and the same time interval was used for both. Sinusoidal-shaped impact loads with a peak value of 2500 kN, and various loading durations, t_L = 2, 4, 6, 8, 80, 100, 120 and 140 ms as shown in Figure 8, were

applied on the pile head. The corresponding relative loading duration, $T_R = t_L/(2L/c)$, varied from about 0.2 to 14.

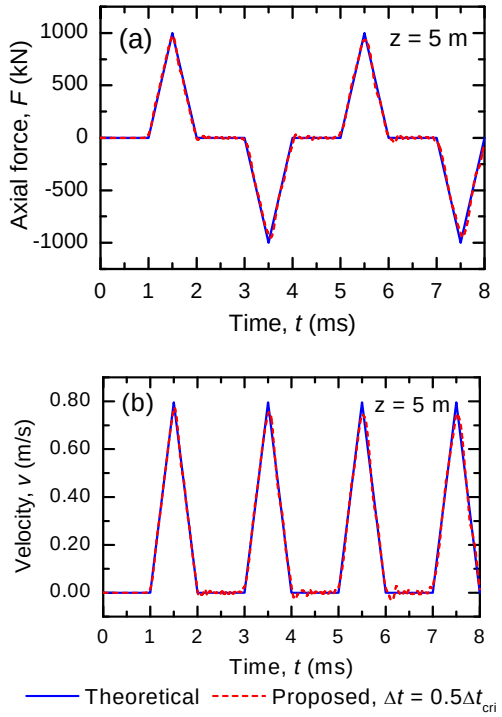

Figure 6 Comparison of the pile response at the middle point of the pile between the proposed method and the theoretical solution: (a) Pile axial force (b) Pile velocity

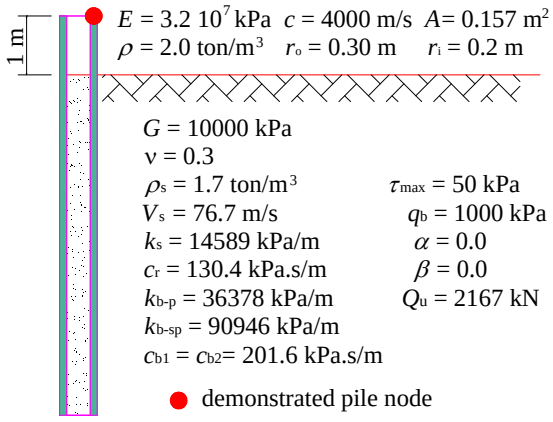

Figure 7 Specifications of the pile and soil

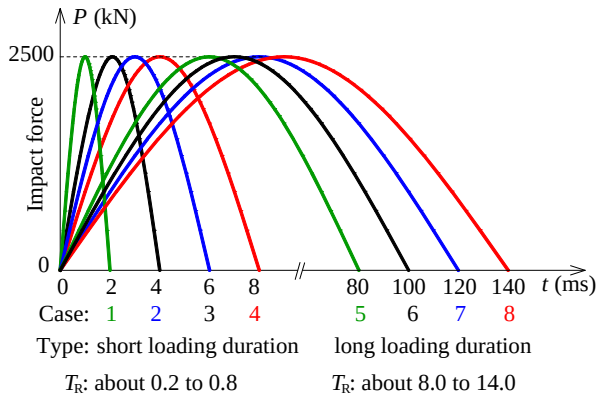

Figure 8 Impact force with different loading durations

Figures 9a and 9b compare the pile head displacements versus time between the proposed and the Smith method for all the loading durations. In the cases with short loading durations, with t_L varying from 2 to 8 ms, as usual in DLTs, the results obtained from the Smith method are comparable with those from the proposed method, although the Smith method tends to slightly underestimate the pile displacement (Figure 9a). In the cases with long loading durations, with t_L ranging from 80 to 140 ms, as usual in RLTs, the results obtained from the proposed method are always greater than those obtained from the Smith method, and this discrepancy becomes larger with the increase in loading duration.

In order to verify the proposed method in more detail, case 6 (t_L = 100 ms) was analysed again using the rigorous method FLAC^{3D} to compare the calculated results with those from the proposed and the Smith methods in the next section.

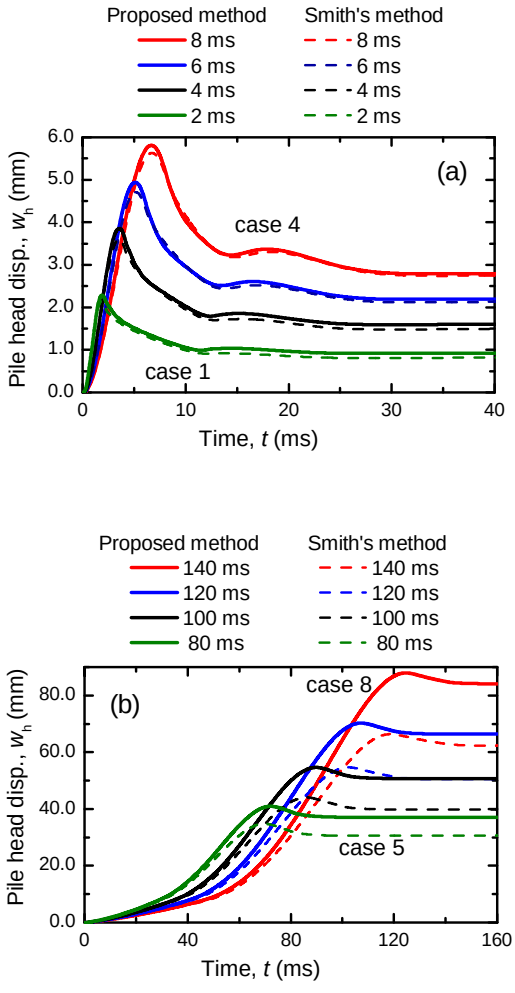

Figure 9 Pile head displacements vs. time: (a) short loading duration (b) long loading duration

2.3.3 Comparison with results calculated using FLAC^{3D}

FLAC^{3D} is a three-dimensional explicit finite difference program for engineering mechanics computation simulating the behaviour of three-dimensional structures constructed on soil, rock or other materials that undergo plastic flow when their yield limits are reached (Itasca, 2002). Materials are represented by polyhedral elements within a three-dimensional grid.

Comparison analyses were made between the proposed method, the Smith method and the FLAC calculation for the case of an open-ended pipe pile. It was assumed that the inside of the pipe pile was filled with soil.

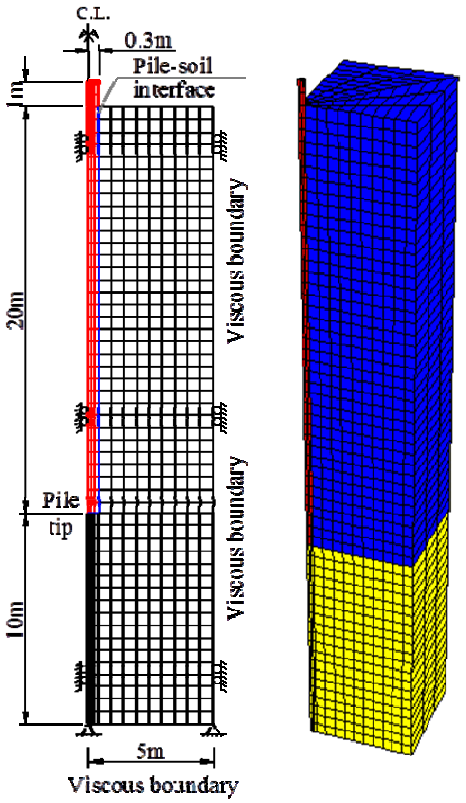

Figure 10 Modelling of the pile and ground using FLAC^{3D}.

Figure 10 shows the numerical model used in FLAC^{3D} to analyse the behaviour of an open-ended pile under vertical dynamic loading. In the present analysis, the pile is modelled by linear elastic elements surrounded by a linear elastic continuum media of soil. To take into account the slippage between the pile and soil, interface elements characterised by Coulomb sliding were employed at the pile-soil interfaces. In order to compare the results from the FLAC^{3D}, the Smith method and the proposed method, a cohesion strength of 50 kPa and the zero friction coefficient were used in the FLAC^{3D} calculations, and $\alpha = 0$ (refer to Eqs. (13) and (14)) and $R_{fs} = R_{fb} = 0$ (refer to Eqs. (17) and (18)) were used in the proposed and the Smith methods.

In the FLAC^{3D} calculations, to minimise the influence of shear waves and longitudinal waves reflected from the outer boundaries of the ground, viscous boundaries were employed in the quarter-symmetry numerical model as shown in Figure 10. The impact load of case 6 (t_L = 100 ms) (see Figure 8) was applied on the pile head.

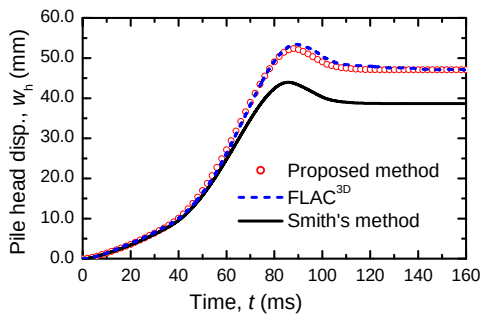

Figure 11 Pile head displacements of the open-ended pile obtained from the three methods

Figure 11 compares the pile head displacement between the proposed method, the Smith method and the FLAC^{3D}. The figure shows that the calculated results obtained from the proposed method agree with those from the FLAC^{3D}, while the Smith method underestimates the pile displacements obtained from the FLAC calculation. That is, if a good matching is obtained using the Smith method, the values of the soil resistance would be overestimated, resulting in overestimation of pile head stiffness and ultimate pile capacity under static loading.

Based on the comparison of the results from three methods, it is obvious that the proposed numerical method is consistent with the FLAC^{3D} and more accurate than the Smith method for a wide range of loading durations. Moreover, the computational time using the proposed method is substantially shorter than the rigorous method, the FLAC^{3D}. In order to obtain the results in Figure 11, for example, the calculation time using the proposed method was only a few seconds while the calculation time using the FLAC^{3D} required more than 30 minutes. Therefore, in terms of precision and computation time, the proposed method is a useful tool in pile driving analysis.

2.3.4 Sensitivity analyses of the example pile driving problem

In order to investigate the sensitivity of the analysed results in pile driving to variation of the soil parameters, the example pile driving problem in Figure 7 with a loading duration of 6 ms (case 3 in Figure 8) was analysed using the proposed numerical method. Since the linear elastic behaviour of the ground is assumed, α values (refer to Eqs. (13) and (14)) and $R_{fs} = R_{fb} = 0$ (refer to Eqs. (17) and (18)) are set as 0 in the example problem, shear modulus and maximum soil resistances are main soil parameters that influence the pile response. Let the values of G, τ_{max} and q_{max} shown in Figure 7 be regarded as the reference soil parameters.

In addition to the analysis with the reference soil parameters (called reference case), twelve cases of analyses were carried out by changing the values of G, τ_{max} and q_{max}. In cases 1 to 4, shear moduli, G, alone were varied, while in cases 5 to 12, τ_{max} and q_{max} were varied. The reference soil parameters were factored from 0.5 to 1.5 in the sensitivity analyses.

It is a common practice in the monitoring of pile driving to measure strains and accelerations near the pile head. Time variations of force, F, velocity, v, and displacement, w, are obtained from these dynamic signals. Hence, the pile responses at the ground level (1 m below the pile head) are compared in this sensitivity analysis. It is well known from the one-dimensional stress-wave theory that the upward travelling force, F_u, is obtained using the following equation.

$$F_u = \frac{1}{2}\left(F - \frac{EA}{c}v\right) \tag{26}$$

where A is the cross-sectional area of the pile.

Calculated pile head displacement and F_u are compared below, because F_u tends to be largely influenced by the soil resistance.

The calculated F_u are shown in Figure 12: (a) in cases 1 to 4 where G alone was varied, (b) in cases 5 to 12 where τ_{max} and q_{max} were varied. It is seen that F_u is very sensitive to the variation of soil resistance, compared to the sensitivity of F_u to the variation of G.

Approximately describing, variation of 5% in the soil resistances causes variation of 20% in F_u while variation of 20% in the shear moduli causes variation of 15% in F_u.

The calculated pile head displacements, w_h, are shown in Figure 13: (a) in cases 1 to 4 where G alone was varied, (b) in cases 5 to 12 where τ_{max} and q_{max} were varied. It is seen that w_h is very sensitive to the variation of soil resistances, compared to the sensitivity of w_h to the variation of G. With a variation of 20% in shear modulus (cases 2 and 3 in Figure 13a), final pile head displacement differs from the reference value by 4%, while only variation of 5% in the soil resistances (cases 8 and 9 in Figure 13b) results in a difference of 8% from the reference value.

Low sensitivity of the dynamic pile responses to the shear modulus, G, may be explained as follows. In pile driving, soil resistance due to radiation damping (velocity-dependent soil resistance) is predominant, compared to static component in the soil

resistance. Hence, maximum soil resistance is mobilised at a very small soil displacement in pile driving, compared to the case of static loading. After the occurrence of the slippage failure at the pile shaft or failure of the ground below the pile tip, the soil resistance predominantly influence the pile response, resulting in low sensitivity of the dynamic pile responses to G.

The calculated static load-displacement curves are shown in Figure 14: (a) in cases 1 to 4 where G alone was varied, (b) in cases 5 to 12 where τ_{max} and q_{max} were varied. As expected, pile head stiffness is sensitive to G, while yield load and bearing capacity are sensitive to the soil resistance.

It can be said from the sensitivity analyses that the results of WMA (dynamic pile responses) are dominantly governed by the assumption of the soil resistance distribution. The soil resistance distribution could be estimated with an acceptable accuracy within a variation of 5 % if the differences between calculated and measured values of the peak upward travelling force and final pile head displacement in WMA are in range of 20 % and 5 %, respectively. Similar criteria could be used in WMA to obtain the distribution of shear modulus with an accuracy of 20 %. If measurements of elastic shear wave velocities, V_s, of the ground are available, we could improve the accuracy of the identified shear modulus from wave matching analysis.

In the following part, the proposed method is used to analyse a case study in Viet Nam for further verification.

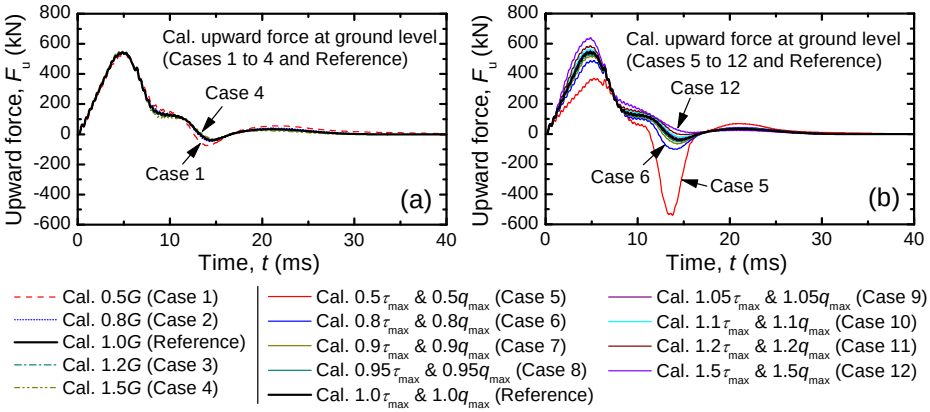

Figure 12 Sensitivity of upward force at ground level due to: (a) Variation of G (b) Variation of τ_{max} and q_{max}

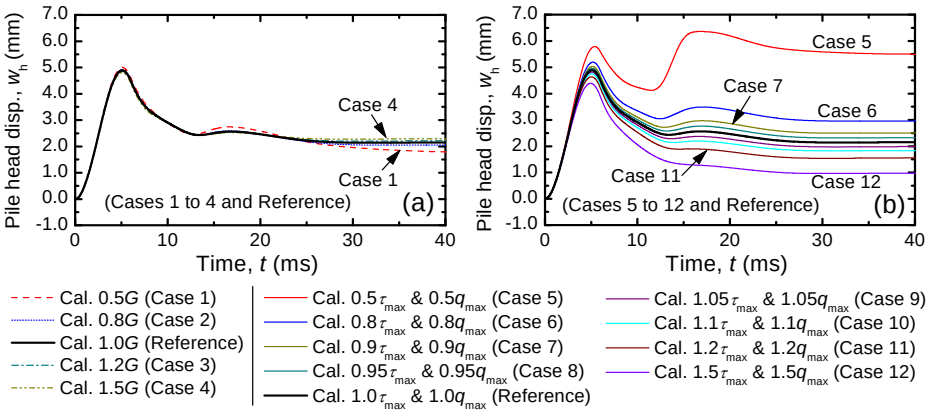

Figure 13 Sensitivity of the pile head displacement due to: (a) Variation of G (b) Variation of τ_{max} and q_{max}

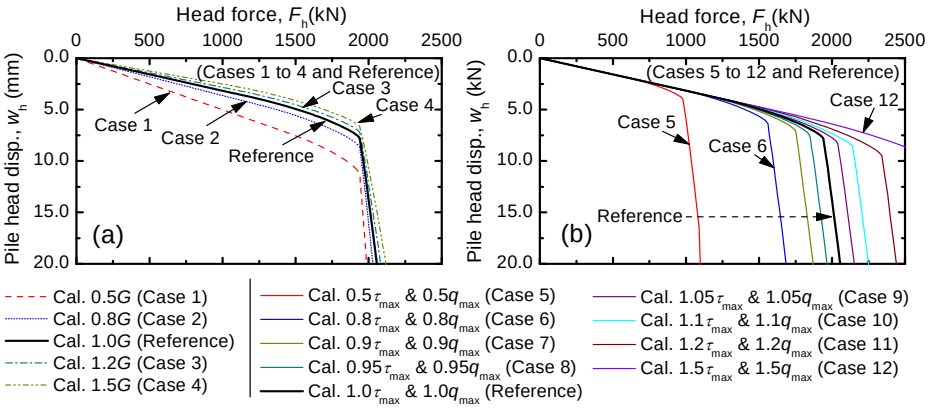

Figure 14 Sensitivity of derived load-displacement curve due to: (a) Variation of G. (b) Variation of τ_{max} and q_{max}

3. A CASE STUDY

In this part, static and dynamic load tests of a spun concrete pile carried out at the Thi Vai international port in Viet Nam (Figure 15) was used to further verify the proposed numerical method.

3.1 Test description

Thi Vai International Port located on the bank of the Cai Mep River in Viet Nam has been completed in 2013. A berth structure, 600 m long and 60 m wide, was constructed in the project as shown in Figure 16. The berth is a quay structure supported by more than one thousand piles. Test piling was conducted at the project site in 2011 to obtain design parameters, to select appropriate driving system, and to seek for driving control and quality assessment methods for constructed piles.

In this site, four test piles were driven prior to construction of the working piles. Two of them were spun concrete piles designated as TSC1 and TSC2, and the other two piles were open-ended steel pipe piles designated as TSP1 and TSP2. The DLTs of TSC1 and TSP1 were analysed and the analysis results have been presented in Phan et al. (2013). In this paper, TSC2 is analysed to further verify the proposed method.

Figure 15 Location of the site with Viet Nam map on the left

Figure 16 Photo of the berth area prior to use

Dynamic load tests (DLTs) were carried out at the end of initial driving (EOD). Re-striking test (BOR) was carried out after a curing periods of 7 days to investigate the "set-up" phenomenon. Static load tests (SLTs) were also conducted after further rest period of 10 days to determine the pile performance and to evaluate the applicability of the WMA to the non-dynamically tested piles.

Geological section at the location of TSC2 is shown in Figure 17. Typically, very soft clay exists from the seabed to depths of 21 m to 28 m. Below this top layer, a clayey sand of about 15 m thick with loose state at the top to medium dense state at the bottom exists, being underlain by hard silt clay that could be regarded as a bearing stratum. The distribution of the SPT *N*-value with depth at the location of the pile was interpolated from the SPT *N*-values of the two boreholes BH21 and BH29 (see Figure 17).

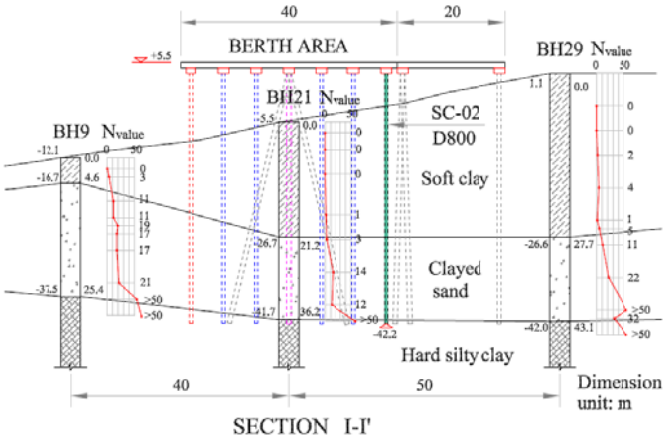

Figure 17 Geological sections at locations of the TSC2

Table 1 Specification of the test pile

Item	Value
Diameter, D (mm)	800
Wall thickness, t_w (mm)	110
Young's modulus, E (kPa)	4.3×10^7
Pile density, ρ (ton/m^3)	2.50
Wave speed, c (m/s)	4148

The pile was driven into the ground using a diesel hammer with mass of 10 tons and a falling height of 2.5 m. After driving the pile was cut to the cut-off level for the dynamic load test. The final seating of the pile is shown in Figure 18.

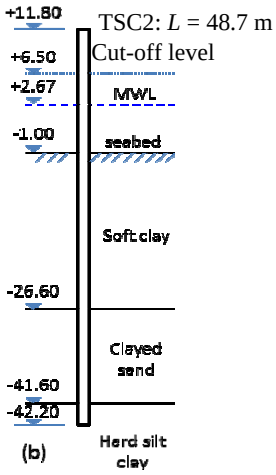

Figure 18 Final seating of the TSC2 at the end of driving

In order to measure signals during DLT, two accelerometers and two strain gauges were mounted symmetrically through the pile axis. Distance from the pile head (the cut-off level) to the strain gauge level was 2.6 m.

3.2 Wave matching analysis (WMA)

3.2.1 Estimation of the initial soil parameters used in WMA

In the WMA, assumptions about the distributions of the outer and inner shaft resistance, and the tip resistance, as well as the shear moduli of the soil layers, are needed.

The soil shear modulus, G_0, at small strain level was estimated

using the following empirical equation proposed by Imai (1977), regardless of soil type.

$$G_0 = 98 \times 120 \times N^{0.737} \quad \text{(kPa)} \tag{27}$$

According to Vietnamese pile design standard code, TCVN 205-1998, the strength parameters, τ_{max} and q_{max}, can be estimated from SPT N-value using the following empirical equations:

$\tau_{max} = 2N$ (kPa) for sand (limit value = 100 kPa) (28)

$\tau_{max} = c_u$ or $10N$ (kPa) for clay (limit value = 150 kPa) (29)

$q_{max} = 300N_p$ (kPa) for both sand and clay soils (N_p is limited to 50) (30)

where N is SPT N-value of the soil surrounding the pile and N_p is the average SPT N-value of the soil at the pile tip within a range of 4D above and 1D below the pile tip.

3.2.3 Modelling of the ground and the pile

Figures 19 shows the profiles of SPT N-values, the soil stratification, location of the pile and the distributions with depth of the shear moduli, G_0, and shear resistances, τ_{max}. Note that the values of G_0 and τ_{max} are the first assumptions of the soil properties estimated from Eqs. (27) to (30) for both outer and inner soils in the WMA.

Although the ground at the location of the test pile consists of three soil layers, it was divided into 5 sub-layers based on the distribution of the SPT N-values. The test pile with the length of 60 m was divided into 60 elements in the analysis. The calculation time step was set at 0.01 ms, about one tenth of critical time step, $\Delta t_{cri} = (\Delta L/c)/2 = 0.1$ ms.

Because the top level of the soil plug was not measured during carrying out the dynamic load test, the soil plug height was assumed to be 70 % to 80 % of the embedment pile length. This assumption is based on the research of Paik et al. (2003) and Paikowsky et al. (1989). Hereafter, the distance from the seabed to the top of the soil plug in the wave matching analysis was assumed to be 9 m, corresponding to about 70 % of the embedment pile length.

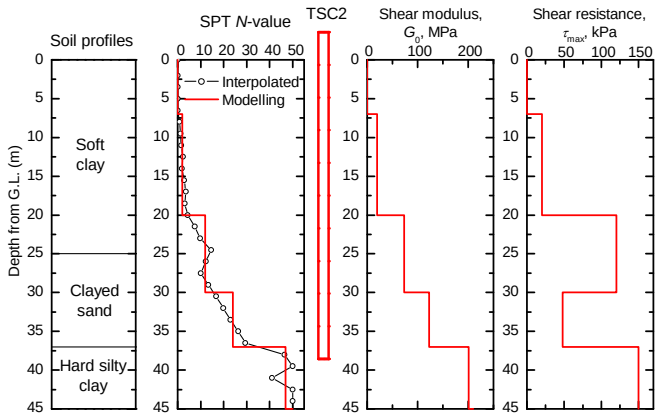

Figure 19 Modelling of the test ground at the test pile TSC2

3.2.2 Estimation of impact head force acting on the pile head

The forces and velocities are usually measured near the pile head, about 1.0 to 2.0 times diameter of the pile. However, in this field tests, distance from the pile head to the strain gauges level, L_m, was 2.6 m, corresponding to 3.25D for the TSC2. In order to model the full pile length in the analysis, it is needed to estimate the impact force acting on the pile head. Since there was no soil resistance from the measurement level to the pile head, the one-dimensional stress-wave theory was employed to calculate the impact force acting on the pile head from the measured force and measured velocity.

The impact head force, $F(0,t)$, is calculated from the measured downward travelling force, $F_d(L_m, t)$, and the upward travelling force, $F_u(L_m, t)$, based on the one-dimensional stress-wave theory, as follows:

$$F(0,t) = F_d(L_m, t + L_m/c) + F_u(L_m, t - L_m/c) \tag{31}$$

in which $F_d(L_m, t+L_m/c)$ and $F_u(L_m, t-L_m/c)$ are calculated from the measured force, F_{meas}, and the measured velocity, v_{meas}, as the following equations:

$$F_d(L_m, t+L_m/c) = \frac{1}{2}\left\{F_{meas}(L_m, t+L_m/c) + \frac{E}{c} v_{meas}(L_m, t+L_m/c)\right\} \tag{32}$$

$$F_u(L_m, t-L_m/c) = \frac{1}{2}\left\{F_{meas}(L_m, t-L_m/c) - \frac{E}{c} v_{meas}(L_m, t-L_m/c)\right\} \tag{33}$$

The calculated impact forces at the pile head in the EOD and BOR tests are shown in Figures 20a and 20b. The measured forces at the strain gauge level are also shown in the figures for comparison.

Under the impact force caused by a hammer mass of 10 ton with a falling height of 2.6 m, the measured settlement per blow of the pile head were 1.30 mm in the EOD test and 0.35 mm in the BOR test. These values along with pile axial force, downward and upward travelling forces, velocities and displacements obtained from the measured dynamic signals at the strain gauge level were used as targets in the wave matching analysis (WMA). In the WMAs, the soil resistance parameters are estimated from the assumed values of the shear modulus and the pile dimensions (refer to Eqs. (2), (3) and (8) to (12)). As for the density, ρ_s, and the Poisson's ratio, ν, of the soils, it was assumed that $\rho_s = 1.73$ ton/m^3 and $\nu = 0.3$.

In the first WMA with the soil properties shown in Figure 19, good matching was not obtained. Then, the soil properties were changed until good matching between the calculated and the measured responses was observed.

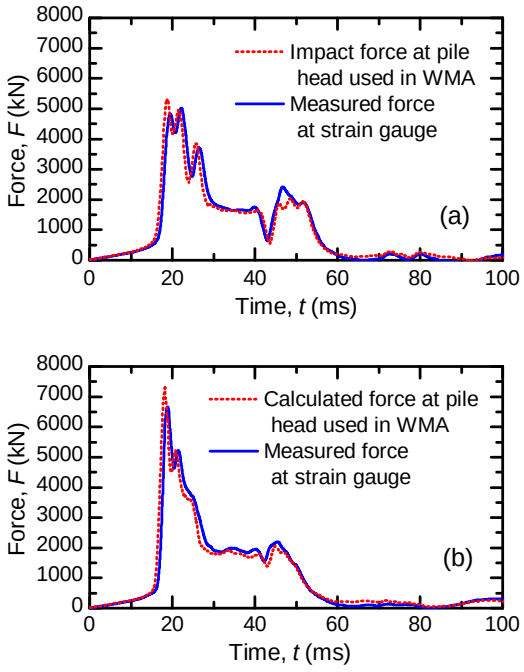

Figure 20 Calculated impact forces at the pile head, together with measured forces of the TSC2 at: (a) EOD. (b) BO

3.3 Results of WMA

Results of the final WMA with consideration of the above discussed criteria at location of the strain gauge including axial forces,

downward and upward travelling forces, velocities and displacements are shown in Figure 21 for the EOD test and in Figure 22 for the BOR test.

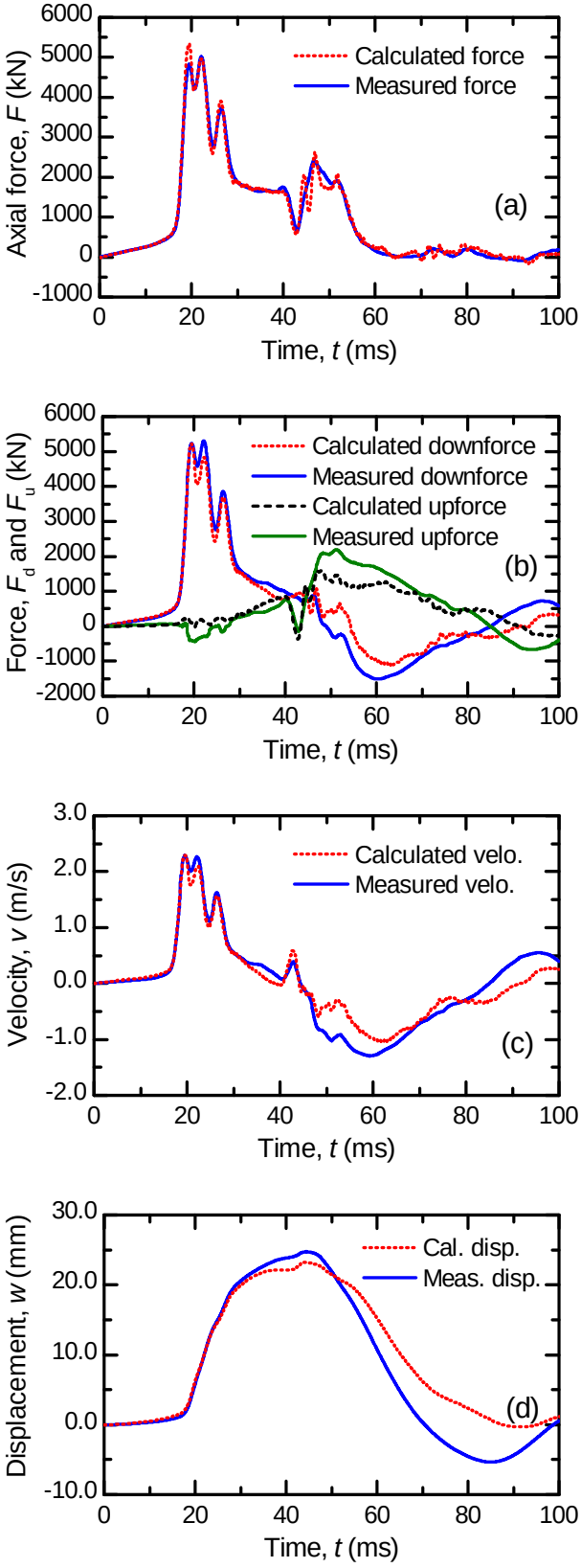

Figure 21 Results of the final WMA in EOD test (a) Force (b) Downward and upward travelling forces (c) Velocity (d) Disp.

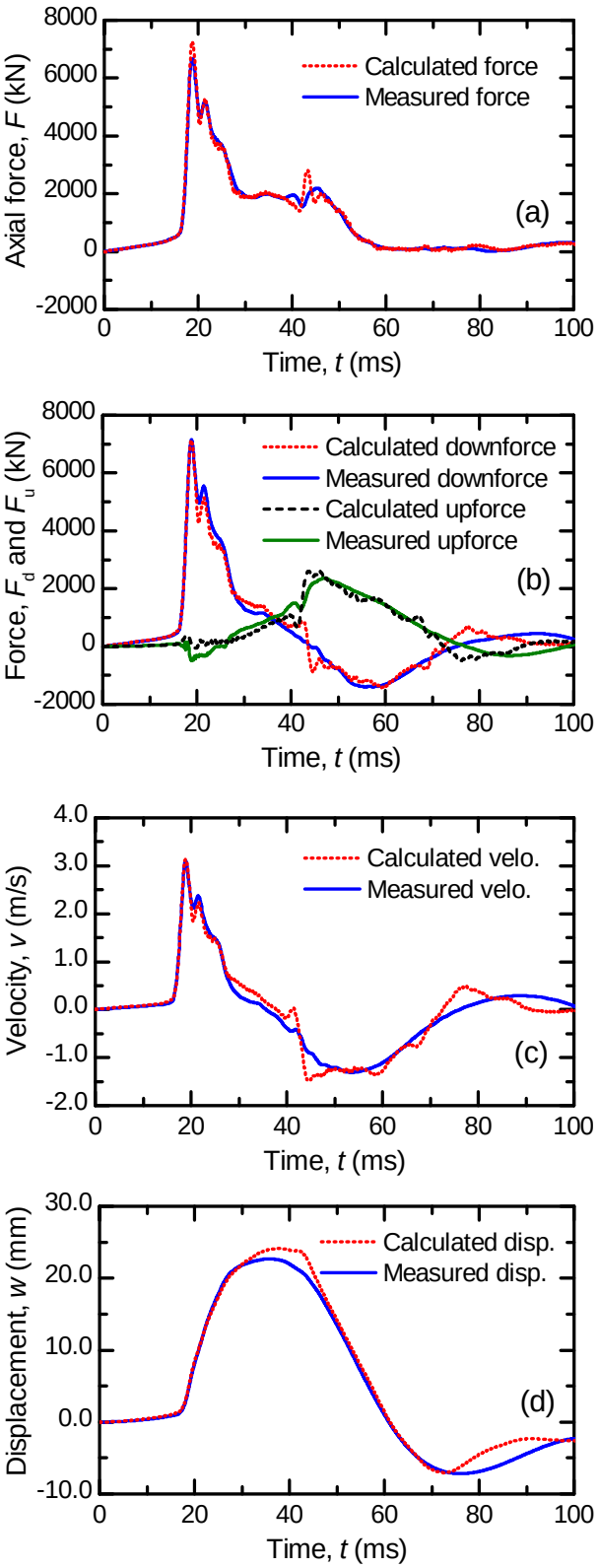

Figure 22 Results of the final WMA in BOR (a) Force (b) Downward and upward travelling forces (c) Velocity (d) Disp.

It is noted that the calculated downward and upward travelling forces shown in Figures 20a and 20b were estimated from the calculated axial force, F, and the calculated velocity, v, at the strain gauge level using Eqs. (32) and (33), respectively.

The soil parameters identified from the final WMA are shown in Figure 23a for the outer soil and in Figure 23b for the inner soil, and indicated in Table 2 for the soil at the pile tip and at the soil plug base. The first assumptions of the soil are also indicated in the figure for comparison.

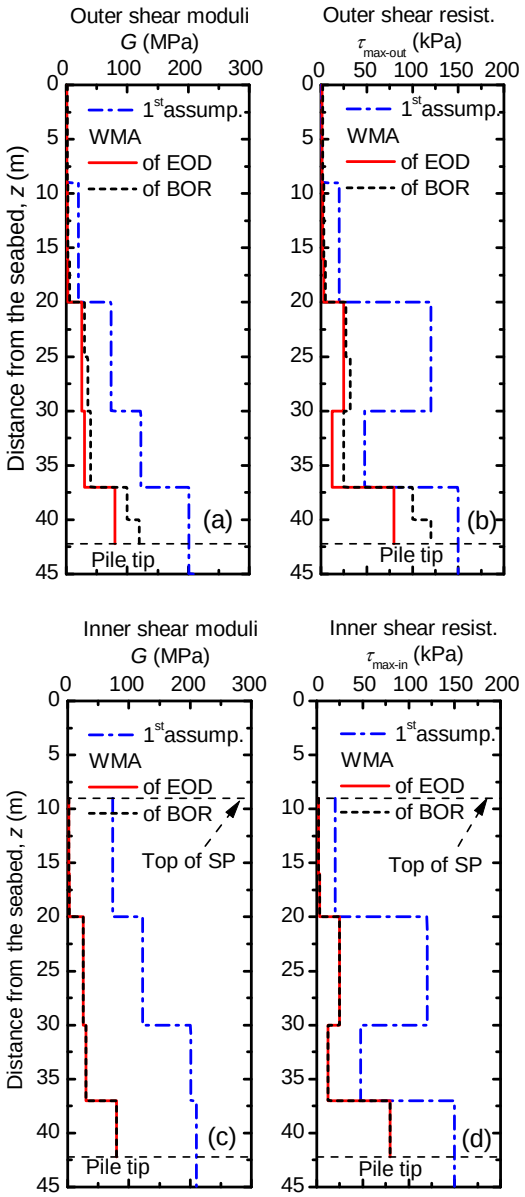

Figure 23 Soil properties obtained from the final WMA of the TSP1 in the EOD and BOR tests. (a) Outer shear modulus (b) Outer shear resistance (c) Inner shear modulus (d) Inner shear resistance

Table 2 The soil parameters at the pile tip and soil plug base identified from the final WMA

Item	Unit	EOD test	BOR test	1st assump.
G_b at the pile tip,	MPa	950	2000	210
G_{sp} at soil plug base,	MPa	200	400	210
$q_{b,max}$ at the pile tip,	kPa	10000	30000	15000
$q_{sp,max}$ at the soil plug base	kPa	3000	3000	15000

The other identified soil parameters are, $\alpha = 0$ (refer to Eqs. (13) and (14)), $R_{fs} = R_{fb} = 0$ (refer to Eqs. (17) and (18)). Note here that WMAs with various values of R_{fs} and R_{fb} were carried out, and it was found that the influence of R_{fs} and R_{fb} is negligible in WMA, because the slip failure at the outer pile shaft and failure of the soil beneath the pile annular base occur by very small soil displacements (= pile node displacements before failure) due to a large amount of damping force. Hence, the soil response is substantially elastic in WMA (in dynamic loading). It may be difficult to identify R_{fs} and R_{fb} from WMA correctly. Appropriate estimation of R_{fs} and R_{fb} may be largely dependent on database of SLTs.

As seen from Figures 23a and 23b, the values of shear modulus, G, and the shear resistance, τ_{max}, of each soil layers identified from the final WMA of the BOR test were greater than those of the EOD test, indicating that the "set-up" phenomenon occurred during the rest period between the EOD and BOR tests. Such phenomenon was also obtained for the soil at the pile tip by comparison of the identified values, G_b and $q_{b,max}$, between the EOD and BOR tests in Table 2.

In both EOD and BOR tests, the first assumption of the shear modulus estimated from empirical equation Eq. (27) were overestimated, compared to the finally identified values (Figures. 23a and 23b). Comparison of the outer shear modulus between the identified values from BOR test and the firstly assumed values suggests that reduction factor of 0.1 to 0.15 for soft soils (the top soil layer of soft clay and the upper part of the second soil layer of clayey sand with loose packing state), 0.15 to 0.30 for medium soils (the upper part of the second soil layer of clayey sand) and 0.30 to 0.45 for hard soils (the lower part of the second soil layer of clayey sand with medium packing state and the third soil layer of hard silt clay) can be used to estimate the shear module of soils at this particular site. In case of shear resistances, the empirical equations (28) and (29) overestimated the identified values for both outer and inner soils while first assumption of end-bearing resistances at the pile tip and at the soil plug base calculated from equation (30) underestimated the identified ones. Hence, it is needed to consider such differences when estimating the ultimate bearing capacity of the pile from SPT N-value.

According to the final WMA results in Figure 23d, the set-up phenomenon of the inner shear shaft resistance was negligible in these particular cases. Hence, it could be thought that the set-up phenomena are mainly caused by the "set-up" phenomenon of the outer shaft resistance.

Figure 24 shows the static load-displacement curves calculated from the soil properties identified in the final WMAs of EOD and BOD tests, compared with the static load test result in two cycles of loading process. The stiffness of the static response derived from the final WMA of the BOR test was higher than that of the static response in the EOD test. As mentioned earlier, BOD test was carried out 7 days after EOD test and SLT was carried out 10 days after BOD test. It may be reasonable that higher pile head stiffness identified from BOD test was caused by set-up" phenomenon of the soil between EOD and BOR tests. Such phenomenon might have continuously occurred from BOR test to SLT test due to the further rest period of 10 days, resulting in higher pile head stiffness at the SLT compared to the BOR test. Another possible reason for the difference between the load-displacements curves measured in SLT and derived from the WMA of BOR test is an imperfect modelling of the soil response used in the analysis. In order to examine the modelling of the soil response in more detail, it is required to carry out SLT just after the end of pile driving so that the influence "set-up" could be neglected. At present, it is difficult to make a definite conclusion for this.

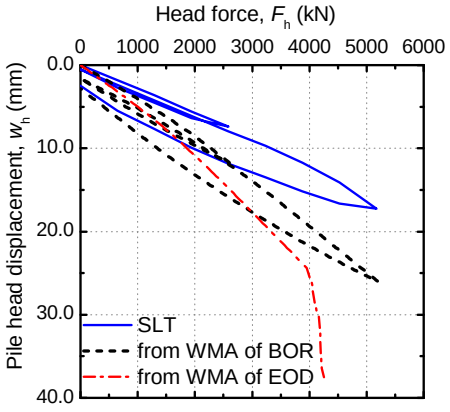

Figure 24 Comparison of static curves of the TSC2

The ultimate pile capacity of 4100 kN was derived from the WMA of EOD test. However, the ultimate capacity was not obtained from the WMA of BOR test, indicating that TSC2 has an ultimate capacity greater than 5200 kN. This result conforms to the SLT result. It is recommended to use a driving hammer having a higher driving energy to obtain the ultimate capacity of the pile after the set-up phenomena.

4. CONCLUSIONS

In this paper, a matrix method using a finite difference scheme to analyse the phenomenon of stress wave propagation in an open-ended pipe pile under both static and dynamic loading conditions has been proposed. In this method, the influence of stress wave propagation in the soil plug was considered, and the no linearity of the soil stiffness and damping coefficient were also taken into account. The proposed method was first verified by comparing the analysed results with those from a theoretical solution, the conventional Smith method, and a rigorous continuum method, the FLAC^{3D}. Second, the static and dynamic load testing of a spun concrete pile in a construction site in Viet Nam were used to examine the applicability of the proposed method to dynamic pile load testing. WMA of the DLTs were conducted to identify the distribution of soil resistance with depth and then to derive the static load-displacement relations.

The following conclusions and findings were drawn from the numerical analyses and the case study with limited conditions:

(1) The results obtained from the proposed method are comparable with those obtained from the rigorous continuum method, the FLAC^{3D}.

(2) The proposed method has a fast computation time when compared to the rigorous method.

(3) It was suggested from the WMAs of EOD and BOR tests as well as the SLT result in the case study that the spun concrete pile driven into clayey ground along the Cai Mep River exhibits a great degree of "set-up".

(4) A large number of WMAs with various distributions of internal and external shaft resistance were conducted to obtain good matching shown in Figures 21 and 22. In order to make the proposed approach be a more practical tool, further research will be needed to explore a more efficient manner of WMA procedure.

Although the validity of the proposed method was examined using the f**u**ll-scale test in this study, analyses of other full scale pile load tests with different pile configurations and soil conditions using the proposed method would be useful for further verification.

5. ACKNOWLEDGEMENTS

The authors would like to express our appreciation to the VIBROBIS- South VietNam Bridge Road Building Technology Institute, Viet Nam, the ANH VU Geotechnical and Civil Engineering Company, and the Penta-Rinkal Joint Venture for permission of using the static and dynamic load test results in this paper.

6. REFERENCES

Bermingham, P. and Janes, M. (1989). An innovative approach to load testing of high capacity piles. Proc. of Int. Conf. on Piling and Deep Foundations, pp. 409-413.

Chow, Y.K. Analysis of vertically loaded pile groups (1986). Int. Jour. for Numerical and Analytical Methods in Geomech., 10, pp. 59-72.

Chow, Y.K. and Smith, I.M. (1984). A numerical model for the analysis of pile drivability. Proc. 2nd Int. Conf. on the Application of Stress waves to Piles, Sweden, pp. 319-325.

Edward, L.W. (2000). Dynamic analysis using numerical integration. Three-dimensional static and dynamic analysis of structures. Computers and Structures, Inc., Berkeley, California, USA, 20.1-20.11.

Goble, G.G. and Rausche, F. (1976). Wave equation analysis of pile driving – WEAP program. FHWA, 1 to 4: FHWA IP-76-14.1 to76-14.4.

Goble, G.G. and Rausche, F. (1979). Pile driveability prediction by CAPWAP. Numerical method in offshore piling, ICE, London, pp. 29-36.

Heerema, E.P. and de Jong, A. (1979). An advanced wave equation computer program which simulates dynamic pile plugging through a coupled mass-spring system. Proc. Int. Conf. on Num. Methods in Offshore Piling, ICE, London, pp. 37-42.

Idriss, I. M. and Seed, H.B. (1969). Seismic response of horizontal soil layers. Journal of the Soil Mechanics and Foundation Division ASCE, 94(SM4), pp. 1003-1031.

Imai, T. (1977). P- and S-wave velocities of the ground in Japan. Proc. 9th ICSMFE, Tokyo, 2, pp. 257-260.

Itasca (2002). Fast lagrangian analysis of continua in three dimensions (FLAC^{3D}), version 3.0. Itasca Consulting Group, Inc. Minesota.

Kusakabe, O. and Matsumoto, T. (1995). Statnamic test of Shonan test program with review of signal interpretation. Proc. of 1st Int. Stanamic Seminar, Vancouver, pp. 113-122.

Liyanapathirana, D.S., Deeks, A.J., Randolph, M.F. (2001). Numerical modelling of the driving response of thin-walled open-ended piles. Int. J. Numer. Anal. Meth. Geomech., 25, pp. 933-953.

Matsumoto, T. and Takei, M. (1991). Effects of soil plug on behaviour of driven pipe piles. Soils and Foundations, 31(2), pp. 14-34.

Matsumoto, T., Wakisaka, T., Wang, F.W., Takeda, K. and Yabuuchi, N. (2004). Development of a rapid pile load test method using a hammer mass attached with spring and damper. Proc. of 7th Int. Conf. on Application of Stresswave Theory to Piles, Selangor, Malaysia, pp. 351-358.

Newmark, N.M. (1959). A method of computation for structural dynamics. Journal of Engineering Mechanics, ASCE, 85 (EM3), pp. 67-94.

Matsumoto, T., Tsuzuki, M. and Michi, Y. (1994). Comparative study of static loading test and Statnamic on steet pipe pile driven in a soft rock. Proc. of 5th Int. Conf. on Exhibition on Piling and Deep Foundations, Bruges, Belgium, 5.3.1-5.3.7.

Middendorp, P. and van Weele, A.F. (1986). Application of characteristic stress wave method in offshore practice. Proc. 3rd Int. Conf. on Numerical Methods in Offshore Piling, Nantes, Supplement, pp. 6-18.

Randolph, M.F. and Simon, H.A. (1986). An improved soil model for one dimensional pile driving analysis. Proc. 3rd Int. Conf. Numerical methods in Offshore Piling, Nantes, pp. 3-17.

Randolph, M.F. and Deeks, A.J. (1992). Dynamic and static soil models for axial response. Proc. 4th Int. Conf. Application of Stress Wave Theory to Piles, The Hague, pp. 3-14.

Smith, E.A.L. (1960). Pile Driving Analysis with the wave equation. Jour. of Soil Mech. and Found. Eng., ASCE, 86, pp. 35-64.

Paikowsky, S.G. and Chernauskas, L.R. (2008). Dynamic analysis of open-ended pipe pile. Proc. 8th Int. Conf. Application of Stress Wave Theory to Piles, Lisbon, pp. 59-76.

Paikowsky, S.G., Whitman, R.V. and Baligh, M.M. (1989). A new look at the phenomenon of offshore pile plugging. Marine Georesources Geotech. , 8, pp. 213-230.

Paik, K., Salgado, R., Lee, J. and Kim, B. (2003). Behaviour of open- and closed-ended piles driven into sand. Journal of Geotech. and Geo-envir. Engineering, ASCE, 129(4), pp. 296-306.

Phan, TL., Matsumoto, T. and Nguyen, HH. (2013). Comparison of Static and Dynamic Pile Load Tests at Thi Vai International Port in Viet Nam. International Journal of Geoengineering Case Histories, 3(1), pp. 36-66.

Wakisaka, T., Matsumoto, T., Kojima, E., Kuwayama, S. (2004). Development of a new computer program for dynamic and static pile load tests. Proc. 7th Int. Conf. on the Appl. of Stress-Wave Theory to Piles, Selangor, Malaysia, pp. 341-350.

TCXDVN 205-1998. Pile foundation- Specifications for design.

Appendix: **FORMULATION OF STIFFNESS, DAMPING AND MASS MATRICES IN THE PROPOSED METHOD**

The substantial forms of the stiffness matrix [*K*], the damping matrix [*C*] and the mass matrix [*M*] for a simple modelling of the pile and soil system (Fig. A1) are given. They are indicated in full matrix forms for easy understanding of the constitution of the matrices. The matrices are symmetric. [*K*], [*C*] and [*M*] have band widths of 5, 7 and 1, respectively. Hence, semi-band matrices having the band width of 7 are used for solving Eq. (24).

At the start of calculation, the values of the springs connected to the plastic sliders, $k_{ii,\,n}$ (interface spring stiffness at inner surface at *n*th node) and $K_{io,\,n}$ (interface spring stiffness at outer surface at *n*th node), are set as very large so that the pile node and the adjacent soils displace together (bonded condition) because the slip failure does not occur at initial step. Once the condition of the slippage is reached at the inner shaft or the outer shaft, the values of $k_{ii,\,n}$ or $K_{io,\,n}$ is set as very small value so that the pile node and the adjacent soil displace independently (unbonded condition). When the condition of re-join of the pile and the soil is achieved, the values of $k_{ii,\,n}$ or $K_{io,\,n}$ are recovered to large value. Similar calculation procedure is employed for the base soil resistance.

As previously mentioned, the same calculation procedure is employed for the analysis of static loading, although the values of [*C*] and [*M*] are set at zero. The resulting plugging mode, perfectly plugged or unplugged mode, is merely dependent on the calculation result. If the potential of the total inner shaft resistance is larger than the soil resistance beneath the soil plug base, the perfect plugging mode is achieved.

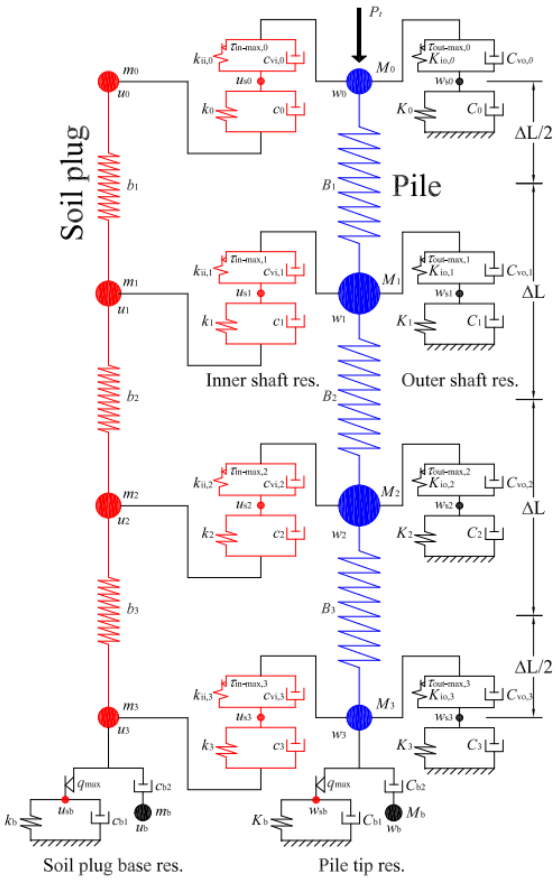

Figure A1 Modelling of the pile and soil system

Stiffness matrix [K]

$\{U\}$	w_0	u_0	w_{s0}	u_{s0}	w_1	u_1	w_{s1}	u_{s1}	w_2	u_2	w_{s2}	u_{s2}	w_3	u_3	w_{s3}	u_{s3}	w_{sb}	u_{sb}	w_b	u_b
w_0	$B_1+K_{io,0}+k_{ii,0}$		$-K_{io,0}$	$-k_{ii,0}$	$-B_1$															
u_0		k_0+b_1		$-k_0$		$-b_1$														
w_{s0}	$-K_{io,0}$		$K_{io,0}+K_0$																	
u_{s0}	$-k_{ii,0}$	$-k_0$		$k_{ii,0}+k_0$																
w_1	$-B_1$				$B_1+B_2+K_{io,1}+k_{ii,1}$		$-K_{io,1}$	$-k_{ii,1}$	$-B_2$											
u_1		$-b_1$				$b_1+b_2+k_1$		$-k_1$		$-b_2$										
w_{s1}					$-K_{io,1}$		$K_{io,1}+K_1$													
u_{s1}					$-k_{ii,1}$	$-k_1$		$k_{ii,1}+k_1$												
w_2					$-B_2$				$B_2+B_3+K_{io,2}+k_{ii,2}$		$-K_{io,2}$	$-k_{ii,2}$	$-B_3$							
u_2						$-b_2$				$b_2+b_3+k_2$		$-k_2$		$-b_3$						
w_{s2}									$-K_{io,2}$		$K_{io,2}+K_2$									
u_{s2}									$-k_{ii,2}$	$-k_2$		$k_{ii,2}+k_2$								
w_3									$-B_3$				$B_3+K_{ib}+K_{io,3}+k_{ii,3}$		$-K_{io,3}$	$-k_{ii,3}$	$-K_{ib}$			
u_3										$-b_3$				$b_3+k_{ib}+k_3$		$-k_3$		$-k_{ib}$		
w_{s3}													$-K_{io,3}$		$K_{io,3}+K_3$					
u_{s3}													$-k_{ii,3}$	$-k_3$		$k_{ii,3}+k_3$				
w_{sb}													$-K_{ib}$				$K_{ib}+K_b$			
u_{sb}														$-k_{ib}$				$k_{ib}+k_b$		
w_b																				
u_b																				

Damping matrix [*C*]

$\{\dot{U}\}$	$\dot{w}_0$	$\dot{u}_0$	$\dot{w}_{s0}$	$\dot{u}_{s0}$	$\dot{w}_1$	$\dot{u}_1$	$\dot{w}_{s1}$	$\dot{u}_{s1}$	$\dot{w}_2$	$\dot{u}_2$	$\dot{w}_{s2}$	$\dot{u}_{s2}$	$\dot{w}_3$	$\dot{u}_3$	$\dot{w}_{s3}$	$\dot{u}_{s3}$	$\dot{w}_{sb}$	$\dot{u}_{sb}$	$\dot{w}_b$	$\dot{u}_b$
$\dot{w}_0$																				
$\dot{u}_0$		c_0		-c_0																
$\dot{w}_{s0}$			C_0																	
$\dot{u}_{s0}$		-c_0		c_0																
$\dot{w}_1$																				
$\dot{u}_1$						c_1		-c_1												
$\dot{w}_{s1}$							C_1													
$\dot{u}_{s1}$						-c_1		c_1												
$\dot{w}_2$																				
$\dot{u}_2$										c_2		-c_2								
$\dot{w}_{s2}$											C_2									
$\dot{u}_{s2}$										-c_2		c_2								
$\dot{w}_3$													C_{b2}						-C_{b2}	
$\dot{u}_3$														c_{b2}+c_3		-c_3				-c_{b2}
$\dot{w}_{s3}$															C_3					
$\dot{u}_{s3}$														-c_3		c_3				
$\dot{w}_{sb}$																	C_{b1}			
$\dot{u}_{sb}$																		c_{b1}		
$\dot{w}_b$													-C_{b2}						C_{b2}	
$\dot{u}_b$														-c_{b2}						c_{b2}

Mass matrix [M]

$\{\ddot{U}\}$	$\ddot{w}_0$	$\ddot{u}_0$	$\ddot{w}_{s0}$	$\ddot{u}_{s0}$	$\ddot{w}_1$	$\ddot{u}_1$	$\ddot{w}_{s1}$	$\ddot{u}_{s1}$	$\ddot{w}_2$	$\ddot{u}_2$	$\ddot{w}_{s2}$	$\ddot{u}_{s2}$	$\ddot{w}_3$	$\ddot{u}_3$	$\ddot{w}_{s3}$	$\ddot{u}_{s3}$	$\ddot{w}_{sb}$	$\ddot{u}_{sb}$	$\ddot{w}_b$	$\ddot{u}_b$
$\ddot{w}_0$	M_0																			
$\ddot{u}_0$		m_0																		
$\ddot{w}_{s0}$																				
$\ddot{u}_{s0}$																				
$\ddot{w}_1$					M_1															
$\ddot{u}_1$						m_1														
$\ddot{w}_{s1}$																				
$\ddot{u}_{s1}$																				
$\ddot{w}_2$									M_2											
$\ddot{u}_2$										m_2										
$\ddot{w}_{s2}$																				
$\ddot{u}_{s2}$																				
$\ddot{w}_3$													M_3							
$\ddot{u}_3$														m_3						
$\ddot{w}_{s3}$																				
$\ddot{u}_{s3}$																				
$\ddot{w}_{sb}$																	M_b			
$\ddot{u}_{sb}$																		m_b		
$\ddot{w}_b$																				
$\ddot{u}_b$																				